Sensing and Bio-Sensing Research 3 (2015) 79–91

Contents lists available at ScienceDirect

Sensing and Bio-Sensing Research

journal homepage: www.elsevier.com/locate/sbsr

Online monitoring of biofouling using coaxial stub resonator technique

N.A. Hoog [a,c,*], M.J.J. Mayer [b], H. Miedema [c], W. Olthuis [a], A.A. Tomaszewska [c], A.H. Paulitsch-Fuchs [c], A. van den Berg [a]

[a] BIOS – The Lab-on-a-Chip Group, MESA+ Institute of Nanotechnology, University of Twente, 7500 AE Enschede, The Netherlands
[b] EasyMeasure B.V., Breestraat 22, 3811 BJ Amersfoort, The Netherlands[1]
[c] Wetsus, Agora 1, Leeuwarden 8900CC, The Netherlands

ARTICLE INFO

Keywords:
Biofouling
Online monitoring
Stub resonator
Modeling

ABSTRACT

Here we demonstrate the proof-of-principle that a coaxial stub resonator can be used to detect early stages of biofilm formation. After promising field tests using a stub resonator with a stainless steel inner conductor as sensitive element, the sensitivity of the system was improved by using a resonator of shorter physical length, implying higher resonance frequencies (and by that a higher frequency range of operation) and improved sensitivity towards dispersion. In addition, the space between inner and outer conductor was filled up with glass beads, thereby exploiting the larger surface area available for biofilm formation.

Analysis of the biofilm and the stub resonator signal, both as function of time, indicates that the sensor allows detection of early stages of biofilm formation. In addition, the sensor signal clearly discriminates between the first stages of biofilm formation (characterized by separated, individual spots of bacterial growth on the glass beads) and the presence of a nearly homogeneous biofilm later on in time. Model simulations based on the transmission line theory predict a shift of the sensor response in the same direction and order of magnitude as observed in the biofouling experiments, thereby confirming the operating principle of the sensor.

1. Introduction

Biofouling, i.e., the colonisation of an interface by a diverse array of organisms, affects surfaces and by that may have detrimental effects on the operation of processes in the field of water technology such as, raw water pre-treatment, drinking water production and distribution, wastewater treatment, industrial water cooling and water quality analysis [1–6].

Because of the high impact of biofouling on process operation and by implication high economic cost, in recent years there has been an increasing interest in developing an on – line sensor able to monitor biofilm formation in real time, especially in an early stage [7–9]. Despite all the efforts to engineer such a sensor, discussed in detail in [10–16], reliable detection technology for (the onset of) biofouling is still lacking.

Existing technologies rely on pressure drop changes [14,17], differential heat transfer [10,19] or differential turbidity [20]. Actually, none of these methods can reliably detect biofouling in an early stage. Changes are detected when it is already too late and the system operation already suffers from serious impairment.

Of all the different detection technologies to track biofouling, actuators that are either acoustic [21], optical [22] or electromagnetic [23] in nature are most reliable and most sensitive [10,24]. A drawback of all these devices is however that the actual detector required is rather expensive whether that is e.g., an optical sensor [25], an analyser for scattering (S) parameters [18] or an impedance analyser [26].

The motivation to develop a new type of biofouling sensor was based, firstly, on the realization that we really need the detection of biofouling in a much earlier stage than currently available and, secondly, to offer a more cost effective alternative for existing technology. In the present study we demonstrate the feasibility of a (flow-through) coaxial stub resonator as a sensitive element of a biofouling sensor. Such resonator systems and their amplitude-frequency or AF response has been characterized, simulated and reported by the authors previously [27–31]. We discuss two different designs of such resonators. The first one has an inner

* Corresponding author at: BIOS – The Lab-on-a-Chip Group, MESA+ Institute of Nanotechnology, University of Twente, P.O. Box 217, 7500 AE Enschede, The Netherlands. Tel.: +31 631077502.
E-mail address: Natalia.Antonyuk@wetsus.nl (N.A. Hoog).

[1] EasyMeasure B.V. participates in the Wetsus program and is involved in commercialization of the technology.

http://dx.doi.org/10.1016/j.sbsr.2014.10.012
2214-1804/

and outer conductor separated by a fluid. The formation of a biofilm on the surface of the inner conductor (and on the surface of the outer conductor but to a much lesser extent) affects the skin effect of the inner conductor as well as the dielectric between inner and outer conductors thereby changing the AF response of the resonator. In the second type of resonator, the space in between both conductors is filled up with glass beads (Fig. 1).

The changes in AF response are caused by both the formation of a biofilm on the surface of the glass beads and the reaction of the inner conductor surface to the amount of nutrients in the feed stream. In this case, the response is more related to an (apparent) change in composition of the feed solution. The sensor geometry and dimensions were designed such that the sensor can be operated at flow conditions that are relevant for process operation in industrial equipment and piping and that the required electronics equipment can be produced in a cost effective way. Additional advantages of our sensor compared to currently existing ones are that it operates as an early warning system and is low in maintenance.

2. Materials and methods

2.1. Sensor description

Fig. 1 shows a schematic outline and the basic elements of a sensor based on a stub resonator coaxial transmission line, discussed in detail previously [27–31].

The resonator itself consists of an inner and outer conductor separated by a fluid of certain dielectric permittivity. A change in this (effective) permittivity of the fluid, e.g., due to a change in fluid composition, will alter the resonator characteristics. Formation of a biofilm on the surface of the inner and/or outer conductor will also change the behaviour (i.e., resonant frequency and quality factor) of the resonator. In general, the system is more sensitive to changes at the surface of the inner conductor than of the outer conductor. Obviously, the larger the surface area covered with biofilm mass, the higher the volume fraction of biofilm dielectric between inner and outer conductor. As explained in a previous study [28], an inner conductor of larger diameter will however not result in a more sensitive sensor, an effect due to stronger converging electric field lines near an inner conductor of smaller diameter. There is however a way to enlarge the effective surface area without compromising the sensor's sensitivity. Surface area enhancement can also be accomplished by filling up the space in between both conductors e.g., with glass beads (see Fig. 1). A schematic cross section of such system is shown in Fig. 3. The formation of a biofilm on the surface of the glass beads (in red) introduces a dielectric permittivity that differs from the permittivity of the glass and the fluid. As a result, the resonant frequency and quality factor (amplitude ratio) shift upon biofouling of the glass beads surface.

2.2. The dielectric properties of a coaxial resonator filled with glass beads covered with a biofilm

The effective dielectric permittivity ε_{eff} and the effective loss tangent $\tan\delta_{eff}$ of a coaxial resonator with multiple concentric layers of different dielectric permittivity has been described in [33,34] and is expressed by:

$$\varepsilon_{eff} = f(\varepsilon_{r1}, \varepsilon_{r2}, \ldots, \varepsilon_{rn}) \quad (1)$$

$$\tan\delta_{eff} = f(\tan\delta_1, \tan\delta_2, \ldots, \tan\delta_n) \quad (2)$$

In an ideal resonator without any losses, the resonance frequency f_{res} of an open ended ($\lambda/4$) and closed end ($\lambda/2$) resonator are given by Eqs. (3a) and (3b), respectively. In this special case, the dielectric constant ε_{re} can be determined directly from Eqs. (3a) and (3b) [27,28].

$$f_{res} = \frac{2n-1}{2\cdot\pi\cdot\sqrt{LC}} = \frac{c\cdot(2n-1)}{4l\sqrt{\varepsilon_{re}\varepsilon_0\mu_{re}\mu_0}} \quad (3a)$$

$$f_{res} = \frac{n}{2\cdot\pi\cdot\sqrt{LC}} = \frac{c\cdot n}{2l\sqrt{\varepsilon_{re}\varepsilon_0\mu_{re}\mu_0}} \quad (3b)$$

where c represents the speed of light in vacuum (m/s), n the order number of f_{res} (Hz), l the length of the resonator (m), μ_r relative magnetic permeability of the dielectric between inner and outer conductors (–), μ_0 the absolute vacuum permeability (H/m), ε_0 the absolute vacuum permittivity (F/m) and ε_{re} the real part of the relative effective dielectric constant. Note that the capacitance C in Eqs. (3a) and (3b) is determined by the real part ε_{re} of ε_r.

For a lossy resonator, polarization and conductivity losses in the dielectric under investigation, as well as resistance losses in the inner and outer conductors, must be taken into account. A detailed model accounting for these losses, essentially based on telegrapher's equations, is explained in [35].

In order to describe the behaviour of the biofouling sensor i.e., a lossy resonator packed with glass beads on which a film of biofouling can grow, the model described in [35] was extended with expressions for both the effective dielectric permittivity ε_r and the effective conductivity of the composite dielectric consisting of glass beads with biofilm, immersed in a feed substrate.

For a lossy dielectric, complex dielectric permittivity can be described as:

$$\varepsilon_r = \varepsilon_{re} - j\varepsilon_{im} \quad (4)$$

where ε_{re} and ε_{im} represent the real and imaginary parts of ε_r, respectively.

The effective loss tangent $\tan\delta_{eff}$ (–), which is a measure for the dielectric losses in the system, is expressed by Eq. (5):

$$\tan\delta_{eff} = \frac{\omega\varepsilon_{im} + \sigma_{eff}}{\omega\varepsilon_{re}} \quad (5)$$

where ε_{im} and σ_{eff} reflect the polarization losses and the conductivity losses in the dielectric, respectively, and $\omega = 2\pi f$ the angular frequency, in rad/s.

In the following, two models for the effective dielectric permittivity of the composite dielectric will be discussed.

For this, we consider the coaxial resonator packed with glass beads with dielectric permittivity ε_{gb} and volume fraction φ_{gb} [–] (see Fig. 3). The glass beads are covered with a biofouling layer with dielectric permittivity ε_l and volume fraction φ_l. The free space in between the beads is occupied by feed substrate with dielectric permittivity ε_m and volume fraction φ_m.

The first model is known as Lichtenecker's logarithmic law and is based on the assumption that the individual components in the mixture are randomly distributed over the total volume of that mixture [34].

According to Lichtenecker's logarithmic law the effective permittivity ε_{ceff} of the (composite) space between inner and outer conductor is given by:

$$\log\varepsilon_{ceff} = \sum_{i=1}^{n}\varphi_i\cdot\log\varepsilon_i \quad (6)$$

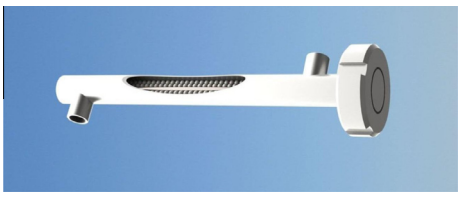

Fig. 1. Schematic 3D image of the coax sensor with a length of 30 cm and an outer conductor diameter of 25.4 mm filled with glass beads. Also indicated are the input and output ports used for fluid flow-through.

$$\log \varepsilon_{ceff} = \varphi_{gb} \cdot \log \varepsilon_{gb} + \varphi_l \cdot \log \varepsilon_l + \varphi_m \cdot \log \varepsilon_m \quad (7)$$

The second model for the effective dielectric permittivity, further on referred to as the "parallel dielectric layers model" is based on the assumption that the resonator is filled with subsequent layers of the individual components of the composite dielectric i.e., with a layer of glass, a layer of biofilm and a layer of feed substrate.

According to the "parallel dielectric layers model" the effective dielectric permittivity ε_{ceff} of the composite space between inner and outer conductor is given by:

$$\varepsilon_{ceff} = \varphi_{gb} \cdot \varepsilon_{gb} + \varphi_l \cdot \log \varepsilon_l + \varphi_m \cdot \log \varepsilon_m \quad (8)$$

The validity of both models for the composite system in Fig. 3 will now be discussed. From an electrical point of view, biofilm formation in a resonator, filled with feed substrate and a packed bed of glass beads as dielectric, can be seen as replacing feed substrate volume by biofilm volume. Therefore, the response changes of the resonator are primarily determined by the difference in dielectric properties of the biofilm and the feed substrate.

However, biofilm formation introduces a third dielectric in the resonator volume and a difference between the biofilm and the feed substrate is that the biofilm preferentially forms on the surface of the glass beads. This is important since the dielectric properties of the composite material in the resonator are not only determined by the volume fraction of the biofilm in the composite material but also by its distribution over the total composite volume. Since a packed bed of glass beads is present between the inner and outer conductors of the resonator, and since biofilm formation preferentially occurs at the glass bead surface, formation of biofilm may result in "thin biofilm sheet structures" throughout the resonator volume, connecting the inner conductor with the outer conductor. However, not all biofilm will be part of a "direct biofilm connection" between inner and outer conductors. A similar reasoning can be held for the packed bed of glass beads.

From the reasoning above, it becomes clear that the system in Fig. 3 cannot be considered as randomly distributed elements of biofilm, glass beads and feed substrate over the total dielectric volume. However, it can also not be considered as a volume filled with subsequent layers of the individual components of the composite dielectric. In reality, the value of ε_{ceff} is expected to be in between the results calculated by model 1 and model 2. In this contribution, both models will be applied as limiting cases to estimate the value of ε_{ceff}.

To calculate the effective loss tangent $\tan\delta_{eff}$ the effective conductivity of the system σ_{ceff} [S/m] was determined assuming that model 2 applies i.e., that the resonator volume is filled with subsequent layers of the individual components of the composite dielectric, resulting in Eq. (9):

$$\sigma_{ceff} = \varphi_{gb} \cdot \sigma_{gb} + \varphi_l \cdot \sigma_l + \varphi_m \cdot \sigma_m \quad (9)$$

This assumption is considered reasonable for estimating σ_{ceff} since the feed substrate is the continuous phase (directly connecting the inner and outer conductors from an electrical point of view) and since it has a high conductivity as compared to the glass beads. This means that the term $\varphi_{gb}\cdot_{gb}$ is negligible in practice as compared to the term $\varphi_{m}\cdot_{m}$. The biofilm is present around the glass beads and its conductivity is also considerably higher than that of the glass beads. Further, as previously explained, "thin biofilm sheet structures" connect the inner and out conductors. So to some extent, the biofilm and feed substrate can be considered indeed to be present in the resonator according to model 2.

2.3. Biofouling formation and structure

In literature, several models on biofilm formation were proposed [8,37–40]. Based on these models we have the following view on biofilm formation in the coaxial resonator system filled with glass beads:

- Almost immediately after bringing the glass beads in contact with feed substrate, containing a suspension of bacteria, its surface is covered by a so-called primary film (conditioning film), modifying the properties of the surface. Formation of such a layer of surface active molecules is the first step prior to the actual formation of the bacterial film and may last for a few seconds to minutes after the glass surface is exposed to the feed substrate [41].
- Primary film formation can be followed by a secondary colonization of bacteria that benefit from a protective environment in the biofilm and/or feed on the remnants of other bacteria. In this secondary community, better resource or space competitors may exclude less competitive organisms [42–44].
- Stable biofilms are composed primarily of microbial cells and extracellular polymeric substances (EPS) secreted by these cells. The EPS fraction consists basically of polysaccharides, accounting for up to 50–90% of the total organic carbon of biofilms and proteins. The polysaccharides can be considered the primary matrix material of the biofilm [45].

For describing the dielectric properties of the biofilm, following assumptions were made:

- The biofilm mainly consists of water i.e., the mass fraction of water in the biofilm is higher than about 0.90 and lower than about 0.98 [46,54–57] and a good approximation of the biofilm is 1000 kg/m^3 [61].
- The real part of relative dielectric permittivity ε_{re} of the viable bacteria and the EPS layer in the biofilm are 60 [52] and 70 [58], respectively.
- Even though the composition of the EPS layers most likely depends on the exact process conditions, its composition was considered to be constant during the course of the experiments of this study. Existing literature report polysaccharides [62] and proteins as dominant EPS components [63].
- According to [52] the overall composition formula of the biomass is expressed by Eq. (10):

$$C : H(1.77) : O(0.49) : N(0.24) \quad (10)$$

2.4. Experimental setups

2.4.1. Half-wave closed ended coaxial resonator

We started out with a half-wave (instead of quarter-wave) closed ended coaxial resonator. This resonator was essentially very similar to the one shown in Figs. 1 and 2 but without the glass beads. Table 1 summarizes the physical dimensions of this stub resonator.

2.4.2. Quarter-wave open-ended coaxial stub resonator

Fig. 4 shows a schematic overview of the experimental set-up used to monitor biofouling. The system comprises three identical flow-through systems, each of them equipped with a peristaltic pump (Masterflex), two tubes and a vessel of 120 L, with pump, tubes and vessel all interconnected to a closed configuration. The construction of the dummies which have the same geometry as a coaxial sensor excluding an inner conductor, the mode of operation and the experimental conditions were also exactly the same as those for the coaxial resonator. These five dummies, all running in parallel with the actual resonator tube, provided five independent controls. This set up made it possible to obtain a control sample each day (up to five) the experiment was running without disturbing the process of biofilm formation in the remaining tubes,

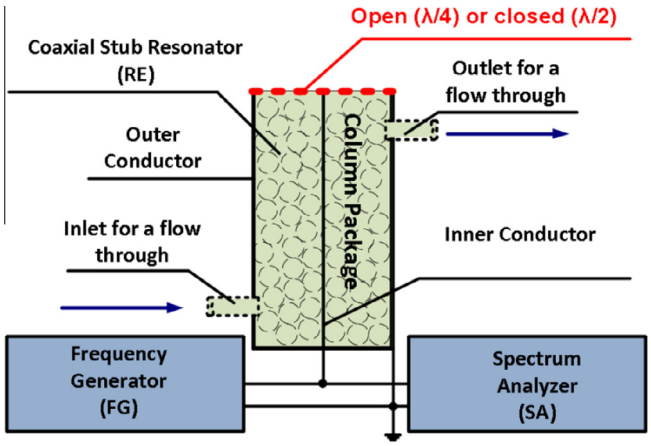

Fig. 2. Schematic outline of the coaxial stub resonator sensing system consisting of a function generator (FG), a spectrum analyzer (SA) and the coaxial stub resonator (RE). The dotted inlet and outlet indicate that the flow-through resonator can be optionally used as batch resonator.

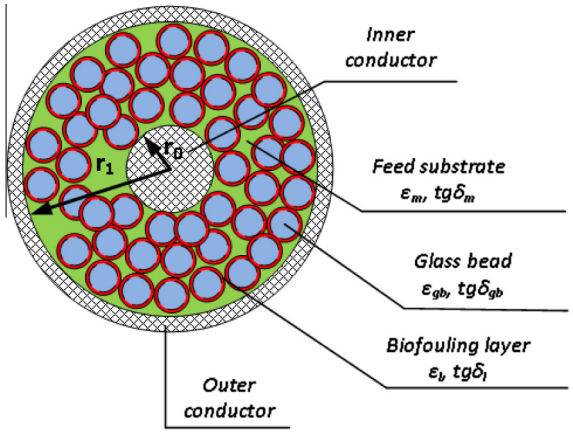

Fig. 3. Schematic cross section of the coaxial stub resonator filled with glass beads of which the surface is covered by a biofouling layer (red). We distinct three types of dielectric between inner and outer conductor: feed substrate (green, dielectric permittivity ε_m (–), loss tangent $\tan\delta_m$ (–), glass beads (blue, dielectric permittivity ε_{gb} (–), loss tangent $\tan\delta_{gb}$ (–) and biofouling layer (red, dielectric permittivity ε_l (–), loss tangent $\tan\delta_l$ (–). (For interpretation of the references to colour in this figure legend, the reader is referred to the web version of this article.)

Table 1
Geometric parameters of the flow-through resonator. The outer and the inner conductors of the resonator were both made from stainless steel 316L.

Parameter	Flow-through resonator
Length, l	1.05 (m)
Inner conductor diameter, d	5×10^{-3} (m)
Inner diameter of the outer conductor, D	75×10^{-3} (m)
Diameters of the fluid inlet and outlet	27×10^{-3} (m)
Conductivity of stainless steel 316L, σ	1.45×10^{6} (S nm^{-1})

including the actual resonator. Feed substrate, 'contaminated' with bacteria cells, was dosed from a supply vessel into each tube by a peristaltic pump at a flow rate of 1.2 L h^{-1}.

Table 2 gives an overview of the dimensions of the quarter-wave coaxial stub resonators applied in this study, see also Figs. 1 and 2.

In order to control variations in the resonance frequency and the shape of a response signal a HAMEG HMS3010 3 GHz Spectrum Analyzer with Tracking Generator was used. (It should be mentioned that this type of Spectrum Analyzer does not have a fixed input voltage of the tracking generator for each piece of equipment. In this study three different Spectrum Analyzer were used (see also MATLAB codes in the "Supplementary information").

The interconnecting transmission lines have all a characteristic impedance Z_0 of 50 Ohm. The transmission lines were connected to the resonator by using SMA (SubMiniature version A) connectors all with a total length of 20 mm.

To prevent corrosion of SMA connectors the sensors were filled with a 1–1.5 cm layer of epoxy resin at the bottom of the sensor, thereby fully immersing the SMA connectors in the resin. The real part of dielectric permittivity ε_{re} of epoxy resin is 3–6 [47].

It should be also mentioned that the difference of the total volume of the dummy and total volume of the resonator with the inner conductor of 5 mm is 4%. This difference in available internal volume is caused by the absence of an inner conductor in the dummies.

The differences in amount of glass beads 14% (the average amount of glass beads in the dummy (resonator without an inner conductor) is 2030 and the average amount in the resonator with an inner conductor 1750).

2.4.3. Feed substrate

In order to enhance bacterial growth the installation was fed with substrate consisting of a solution of $NaCH_3COO$, $NaNO_3$ and NaH_2PO_4 in tap water, resulting in a mass ratio C:N:P of 100:20:10 [46]. All chemicals were purchased in analytical grade (Boom B.V., Meppel, Netherlands) and dissolved in tap water. For the simulations, the value of ε_m of the feed substrate was set at 78 (see also the MATLAB code in the "Supplementary information").

2.4.4. Glass beads

The coaxial resonator tubes and dummies, all with a volume of 137.4 ml, were packed with glass beads of 4 mm diameter (Merck KGaA, Germany), with a total number of beads per tube of, on average, 2030. The surface area of a single glass bead is 0.5 cm^2. The dielectric permittivity of glass ε_{gb} varies within a range of 3.8–19 [48–50]. The dielectric permittivity of quartz glass is 3.8 and that of regular window glass 7.6. Taking into account that the porosity of glass beads is less than that of regular window glass, in this study ε_{gb} was assumed to be 5.8 (see also MATLAB codes in the "Supplementary information").

2.4.5. Culture of Escherichia coli

Escherichia coli (*E. coli*) O157:H7 was cultured by incubating 200 ml standard Lysogeny broth (LB) media for 24 h at 36 °C [49]. The total cell number in the feed substrate solution at the start of the experiment was in the range of 5×10^5 and 10×10^5 cells ml^{-1}.

2.4.6. Sampling and analysis of glass beads

To determine the composition and the amount of accumulated biofouling as function of time, samples of the glass beads from the (dummy) resonator tubes and from the feed substrate (30 ml) were taken during each day of the experiment. Collected beads and sampled feed substrate were stored (at −20) in (disinfected) glass tubes until further investigation. Both types of samples were subjected to four different analyses: TCN, ATP, TOC, HPC, explained in more detail in the following paragraphs.

2.4.7. Total cell number (TCN)

For TCN determination, a Neubauer Improved Counting Chamber was used and the total number of cells in the sample was counted optically using a microscope (DM750, Leica, Wetzlar, Germany). Five squares, each with a volume of 1 μL, were

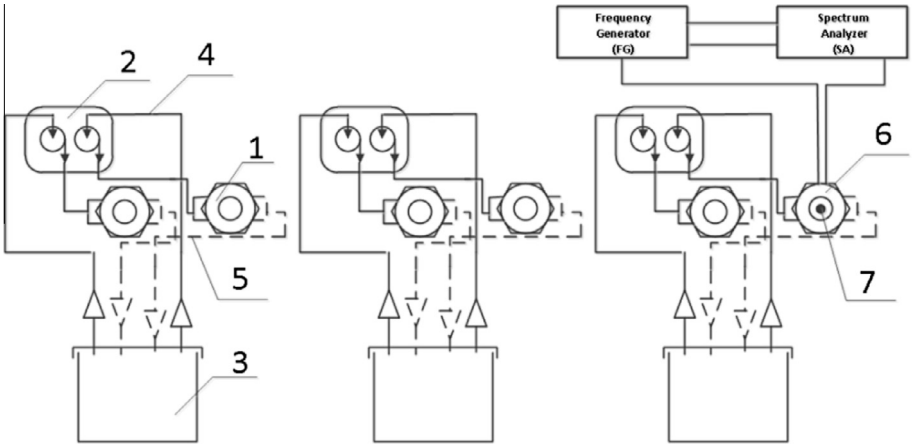

Fig. 4. Schematic of the experimental set-up consisting of (1) dummy (tube), (2) pump with double rotating shaft, (3) tank with feed substrate, (4) inlet hose, (5) outlet hose, (6) coaxial sensor connected to the frequency generator and spectrum analyzer, (7) an inner conductor of coaxial sensor.

Table 2
Geometric parameters of the flow-through resonator (see also the "Supplementary information"). The outer and the inner conductors of the resonator were both made from stainless steel 316L.

Parameter	Flow-through resonator
Length, l	29×10^{-1} (m)
Inner conductor diameter, d	5×10^{-3} (m)
Inner diameter of the outer conductor, D	25×10^{-3} (m)
Diameters of the fluid inlet and outlet	27×10^{-3} (m)
Conductivity of stainless steel 316L, σ	1.45×10^{6} (S m^{-1})

subjected to counting and the average value of two independent duplo measurements was taken. TCN [cells/μL] is given by:

$$\text{TCN} = \text{Number of cell counted/Number of squares} \times \text{counted (mm}^2\text{)} \cdot \text{Depth (mm)} \cdot \text{Dilution factor} \quad (11)$$

2.4.8. Adenosine triphosphate (ATP)

As a relative measure for the active biomass content of the biofilm, the ATP concentration of the biofilm obtained from the glass bead surface was determined. For this purpose, the entire tube volume, containing all 2030 glass beads, was added to 100 ml of phosphate-buffered saline (PBS) solution (containing NaCl 8 g L^{-1}, KCl 0.2 g L^{-1}, $Na_2HPO_4{\cdot}7H_2O$ 1.15 g L^{-1} and KH_2PO_4 0.2 g L^{-1}; pH-adjusted to 7.3). In order to detach the biofilm from the glass bead surface, the suspension of glass beads in PBS was sonicated at 37 kHz for 5 min. After sonication, the suspension was further homogenized using a Vortex (Heidolph Reax Vortex Mixer, Germany). Finally, the suspension was centrifuged for 20 s at 2500 rpm. 20 ml of the supernatant was stored at −20 °C until further analysis by the Vitens laboratory in Leeuwarden (Exp. No. V131232127_F001).

The ATP measurement of the feed substrate was based on 150 ml samples, without further dilution.

2.4.9. Total organic carbon (TOC)

To determine the TOC content of the biofilm, all 2030 glass beads of a single tube were added to 100 ml of PBS in a TOC-free glass tube. Subsequently, the samples were sonicated at 35 kHz for 15 min (BANDELIN, Ultrasonic bath SONOREX DIGITEC, Germany). As for the feed substrate, 150 ml was mixed with 100 ml PBS in a TOC-free glass tube. The TOC concentration in both samples was measured with a TOC analyser (Shimadzu, Japan).

2.4.10. Heterotrophic plate counts (HPC)

100 ml PBS was added to 150 ml of glass beads (containing 2030 beads) and shaken for 20 min. Samples were diluted 10^3, 10^6 and 10^8 times using 2 mm sterile polypropylene tubes. To determine CFU per cm^2, LB agar plates were used. Therefore, 100 μL of diluted sample was spread on the plates. Plates were incubated at 37 °C for 72 h.

The HPC procedure for the feed substrate (105 ml) was essentially the same.

2.5. Experimental conditions

Temperature, conductivity, and operation time were controlled and stable for each set of experiments.

Table 3 contents information regarding experimental conditions.

3. Results and discussion

In presenting the results we will follow the chronological order the sensor has been developed. This way the reader can witness the different phases of the project and, more importantly, follow the arguments that defined our research direction.

Starting point was a flow through half-wave closed ended resonator as shown in Fig. 2 but without the glass beads. In the absence of glass beads the system solely monitors biofilm formation at the surface of inner and outer conductor, both made from (corrosion-resistant) stainless steel. As explained earlier, the resonator is much more sensitive to biofilm formation on the inner conductor as compared to the outer conductor. In a previous contribution [27,28], the authors have shown that such flow-through resonator can be operated in a stable and reproducible way and that it is feasible for measuring the dielectric properties of fluids.

Fig. 5 shows the results of a field test at a drinking water production facility and water quality centre of WLN at Glimmen, Netherlands. The field test was executed at the SenTec testing facility of WLN where different qualities of drinking water are available for testing sensors at "real life conditions". The test was executed with drinking water from Annen i.e., purified ground water.

Even though we monitored biofilm formation for as long as 14 days, the results indicate minimal effects on the AF response. However, visual inspection of both inner and outer conductors revealed surface modification. Both inner and outer conductors of the flow through sensor were covered by a thin but visible slimy layer.

Table 3
Temperature T (°C) and conductivity σ (S/m) of the feed substrate for each set of experiment.

Main points of the experiment	Temperature T (°C)	Conductivity σ (S/m)
WLN at Glimmen, The Netherlands: drinking water from Annen i.e., purified ground water (Fig. 5)	9.6 ± 1.0	$300 \times 10^{-4} \pm 54 \times 10^{-4}$
WLN at Glimmen, The Netherlands: the mixture of drinking water "De Punt" and raw ground water, creating a high iron (hydroxide) content and with that, a high fouling rate (Fig. 6)	10.3 ± 1.5	$300 \times 10^{-4} \pm 54 \times 10^{-4}$
WETSUS, The Netherlands: tap water (Fig. 7)	20.0 ± 1.5	$515 \times 10^{-4} \pm 20 \times 10^{-4}$
WETSUS, The Netherlands: using the substrate of the feed and *E. coli* culture (Fig. 8)	20.0 ± 1.5	$618 \times 10^{-4} \pm 20 \times 10^{-4}$
WETSUS, The Netherlands: using the substrate of the feed, *E. coli* culture and $AgNO_3$ (Fig. 14)	22.0	620×10^{-4}

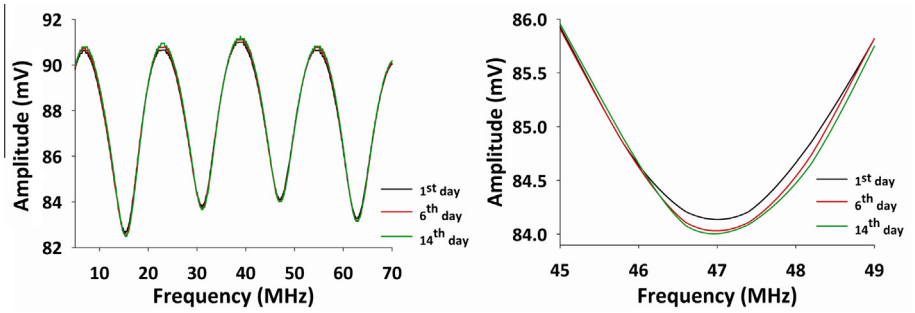

Fig. 5. Left and right panels show the amplitude versus or AF plots in the presence of biofilm on the surface of inner conductor during 12 days of operation using water from Annen in frequency range of 5–70 MHz and the 3rd resonance in more detail, respectively.

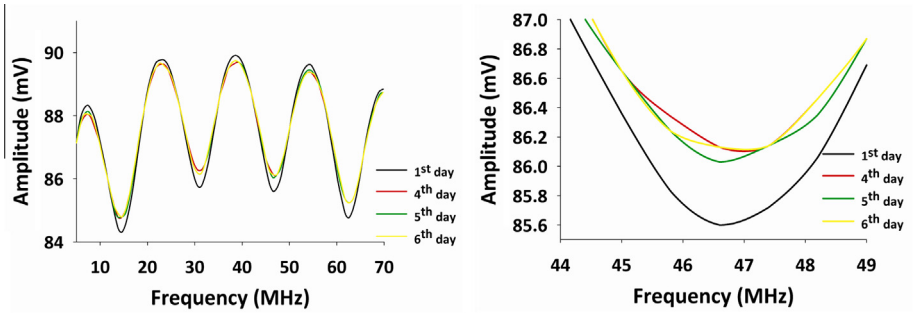

Fig. 6. Left and right panels show the amplitude versus frequency or AF plots in the presence of iron oxide on the surface of inner conductor during 6 days of operation using water from "De Punt" mixed with ground water in frequency range of 5–70 MHz and the 3rd resonance in more detail, respectively.

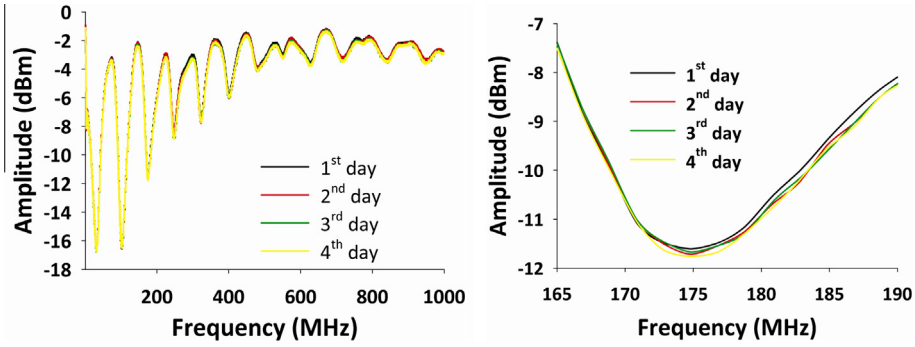

Fig. 7. Left and right panels show the amplitude versus frequency or AF plots in the presence of biofilm on the surface of inner conductor during 4 days of operation using the substrate of the feed and *E. coli* culture in frequency range of 1–1000 MHz and the 3rd resonance in more detail, respectively.

Although the observed lack of signal change in Fig. 5 might be caused by the limited fouling potency of the drinking water used for these experiments, it was concluded that the sensor should be sufficiently sensitive to detect the thin but visible biofilm that was observed after 14 days. In order to obtain more information on the sensor performance under field conditions, it was decided to expose it to water with much higher fouling capacity. For this purpose, the field test was executed with a mixture of drinking water from location "De Punt", i.e., purified surface water, and raw ground water. Now, a clear signal shift was observed within just four days of operation (Fig. 6).

However, afterwards inspection and analysis of the resonator proved a response due to the deposition (scaling) of iron oxide on the inner conductor rather than biofilm formation. This

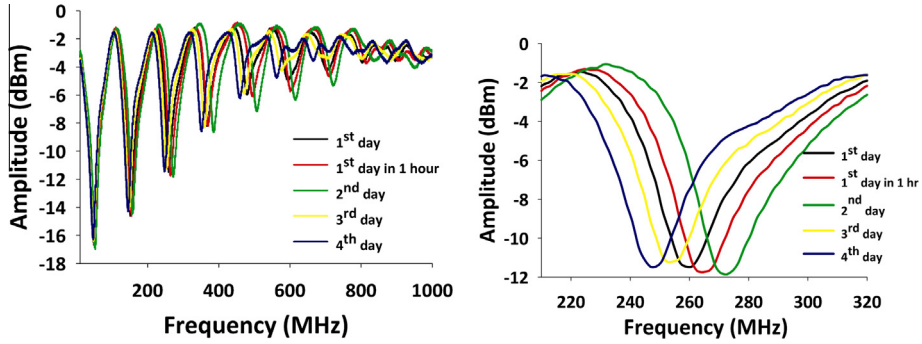

Fig. 8. Left and right panels show the amplitude versus frequency or AF plots in the presence of biofilm on the surface of inner conductor and glass beads during 4 days of operation using the substrate of the feed and *E. coli* culture in frequency range of 1–1000 MHz and the 3rd resonance in more detail, respectively.

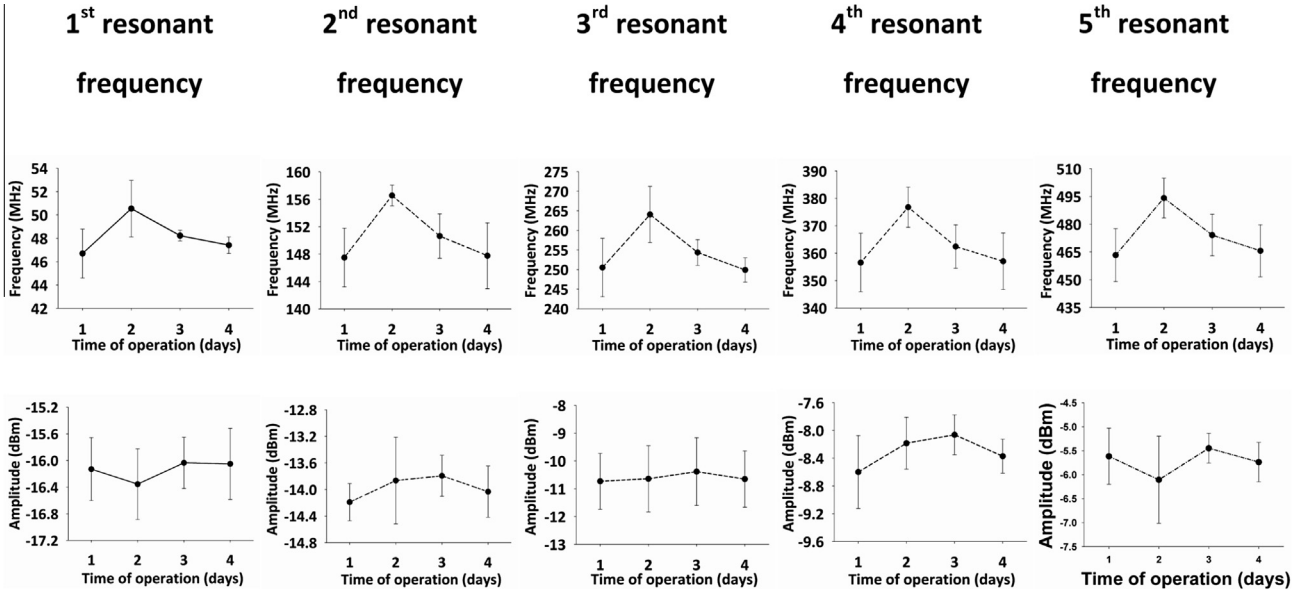

Fig. 9. Resonant frequencies and amplitudes of the first five resonances over a time period of 4 days and in response to biofilm formation. Error bars represent the standard deviations of three independent experiments.

observation actually pointed us in the direction of quite another application for our sensor, i.e., the monitoring of scaling and oxidation process [29].

In order to evoke biofilm formation, our next step was to incubate the system with *E. coli* and perfuse the resonator with a (standard) feed solution promoting bacteria growth. The key adjustment was however to fill the resonator tube with glass beads to enhance the surface area for bacteria adherence.

To show the effect of the presence of glass beads, we run two experiments in parallel, one without (Fig. 7) and the other with glass beads (Fig. 8).

Clearly, the presence of glass beads significantly increased the response sensitivity of the resonator to biofilm formation. This is reflected in the change of both resonant frequency and ratio of current amplitude. The results confirm the hypothesis that the AF responses mainly depend on the formation of biofouling on the surface of glass beads and less depend on multiplication of bacterial cells (*E. coli* in this study) in the feed substrate (see also the earlier). There is also growth of bacteria during biofilm formation. Note that the response shown in Fig. 8 is entirely different from the 'scaling' response shown in Fig. 6. Whereas deposition of $Fe(OH)_3$ results in an upward shift of the AF response i.e., towards a higher amplitude at the resonance frequency, biofilm formation shifts the response, first, towards higher resonance

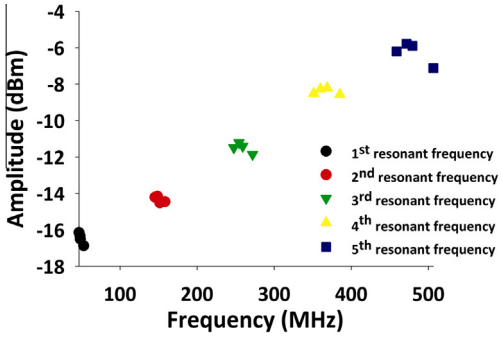

Fig. 10. Correlation between changes in resonant frequencies and amplitude for the first five resonances over a time period of four days and in response to biofilm formation.

frequencies and slightly lower amplitudes, followed by a shift in opposite direction.(discussed later in more detail). This difference points to a different working mechanism responsible for the two different types of responses observed.

Fig. 9 delineates the changes of resonant frequency and amplitude ratio separately for the first five resonances in Fig. 8. The experiments ran for four days and each plot has a data point for

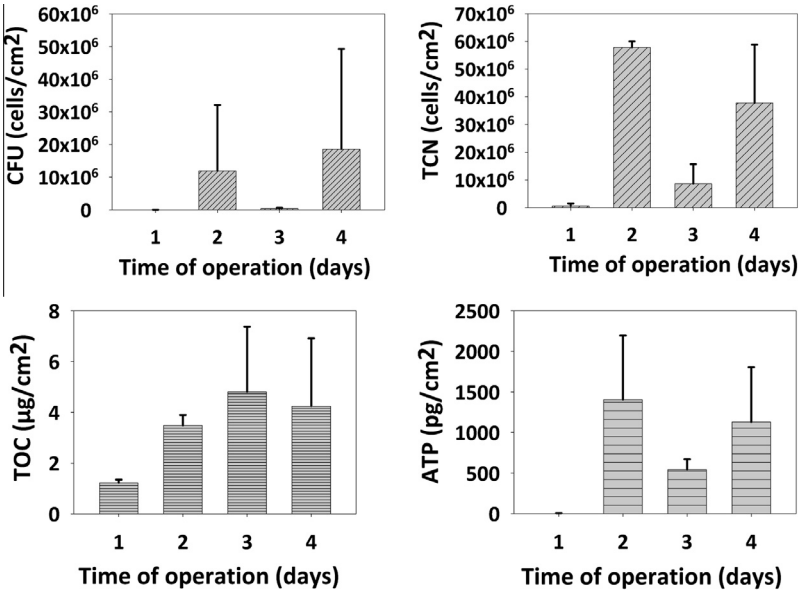

Fig. 11. Analysis of colony forming units (CFU); total cell number (TCN); total organic carbon (TOC) and adenosine triphosphate (ATP) over time and normalized for surface area. All samples used were collected exclusively from biofilm material on the surface of glass beads. Data based on three independent experiments.

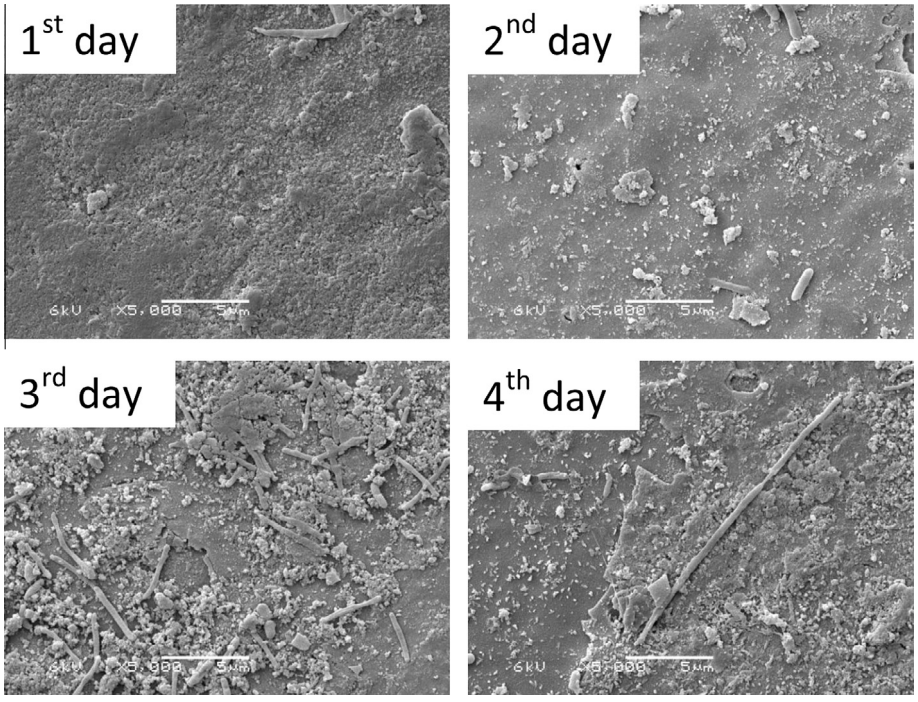

Fig. 12. SEM images of the glass bead surface, taken on 1st, 2nd, 3rd and 4th day of the experiment. Each image gives a qualitative reflection of the observed glass bead surface texture and was selected based on a microscopic scan of different surface areas.

Table 4
The calculated biofilm volume fraction in the dielectric between inner and outer conductors φ_l at days 1–4 as derived from TOC measurements, assuming mass fractions (%) of biomass in the biofilm of 2%, 5% and 10%, respectively (see also the "Supplementary information").

Day	TOC_lab (mg/ml)	2% (w/w) biomass in biofilm	5% (w/w) biomass in biofilm	10% (w/w) biomass in biofilm
1	1.57 ± 0.36	$1.38 \times 10^{-1} \pm 3.13 \times 10^{-2}$	$5.53 \times 10^{-2} \pm 1.25 \times 10^{-2}$	$2.76 \times 10^{-2} \pm 6.26 \times 10^{-3}$
2	3.29 ± 1.11	$2.90 \times 10^{-1} \pm 9.81 \times 10^{-2}$	$1.16 \times 10^{-1} \pm 3.92 \times 10^{-2}$	$5.80 \times 10^{-2} \pm 1.96 \times 10^{-2}$
3	4.32 ± 2.75	$3.81 \times 10^{-1} \pm 2.42 \times 10^{-1}$	$1.52 \times 10^{-1} \pm 9.69 \times 10^{-2}$	$7.62 \times 10^{-2} \pm 4.84 \times 10^{-2}$
4	4.16 ± 2.35	$3.67 \times 10^{-1} \pm 2.07 \times 10^{-1}$	$1.47 \times 10^{-1} \pm 8.29 \times 10^{-2}$	$7.34 \times 10^{-2} \pm 4.14 \times 10^{-2}$

each day. As can be seen, the changes over time for the resonances were very similar, notably in the case of the resonant frequency with a peak value at day 2. The similarity is valid for the amplitude ratio as well (but to a slightly lesser extent) and with a minimum value at day 2. From these similarities in response changes we conclude that the mechanism responsible is the same for each resonance. An important conclusion as it declassifies other, possible interfering, processes causing similar changes.

Fig. 10 correlates the observed change in resonant frequency and the one in amplitude, for the first five resonances and over a time period of four days. The increasing dispersion at higher frequencies (resonances) is evident as the individual data points for each resonance diverge with increasing resonance number. This conclusion is in line with decrease of the quality factor i.e., the broader band with of each resonance relative to its center frequency, with increasing resonance number in the AF plot, see the left panel of Fig. 8.

In order to correlate the observed AF responses of the resonators to bacterial growth/biofilm formation, samples were taken simultaneously and used for total organic carbon (TOC), total cell number (TCN), colony forming units (CFU) and adenosine triphosphate (ATP) analysis (Fig. 11; $n = 3$). The increase of TOC over time, obtained exclusively from the bead surface, demonstrates the 'deposition' of carbon. The observation that TCN and ATP simultaneously increase renders support for the conclusion that the increase of TOC reflects the presence of (living) bacteria on the bead surface rather than scaling effects due to the deposition of inorganic carbon. The temporal dip at day 3 seen simultaneously in the analysis of ATP, TCN and CFU indicates a 'real' effect rather than an artefact. The most plausible reason for this observation is carbon depletion of the feed solution (experiments were performed in a closed system at recycle conditions over the resonators and dummies). The carbon coming free after mass starvation of bacteria cells served as carbon source, resulting in a blooming bacteria culture at day 4.

In addition to the CFU, TCN, TOC and ATP measurements, the glass bead surface was examined by scanning electron microscopy (SEM) and examples are shown in Fig. 12, at magnifications of 5000. The SEM images indicate attachment of biofilm after day 1 but, in addition, also some detachment of biofilm between days 3

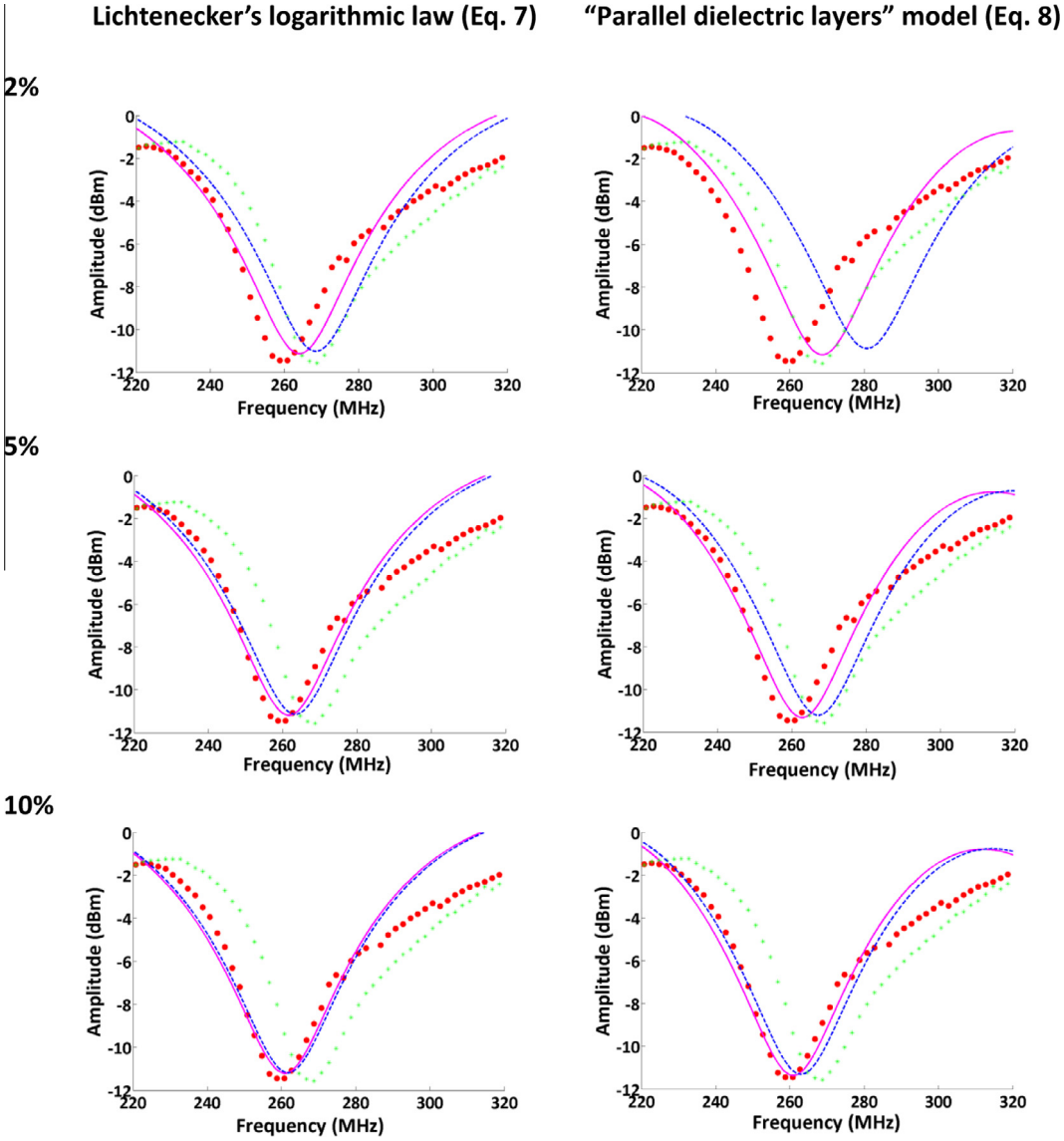

Fig. 13. The observed and simulated third resonance AF plots for the biofouling experiments comprising the resonators filled with glass beads. The experimental data for days 1 and 2 are represented by the red circles and green circles, respectively. The magenta and blue curves represent the model simulations for the first day and second day respectively. (For interpretation of the references to colour in this figure legend, the reader is referred to the web version of this article.)

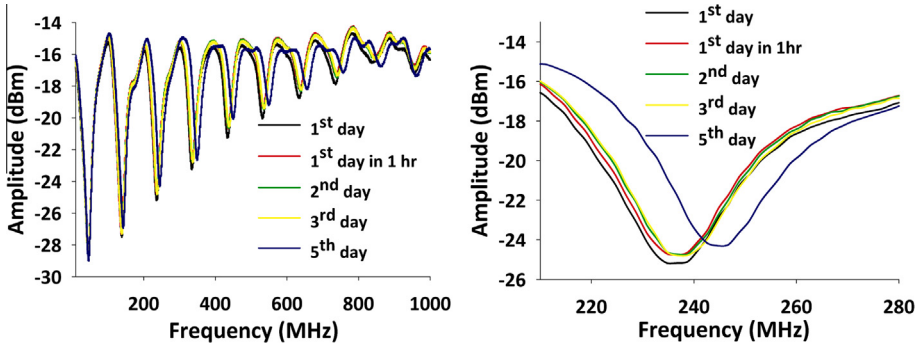

Fig. 14. AF response in the presence of 3 mM $AgNO_3$ during 5 days of operation in frequency range of 1–1000 MHz with the 3rd resonance plotted in more detail (right panel).

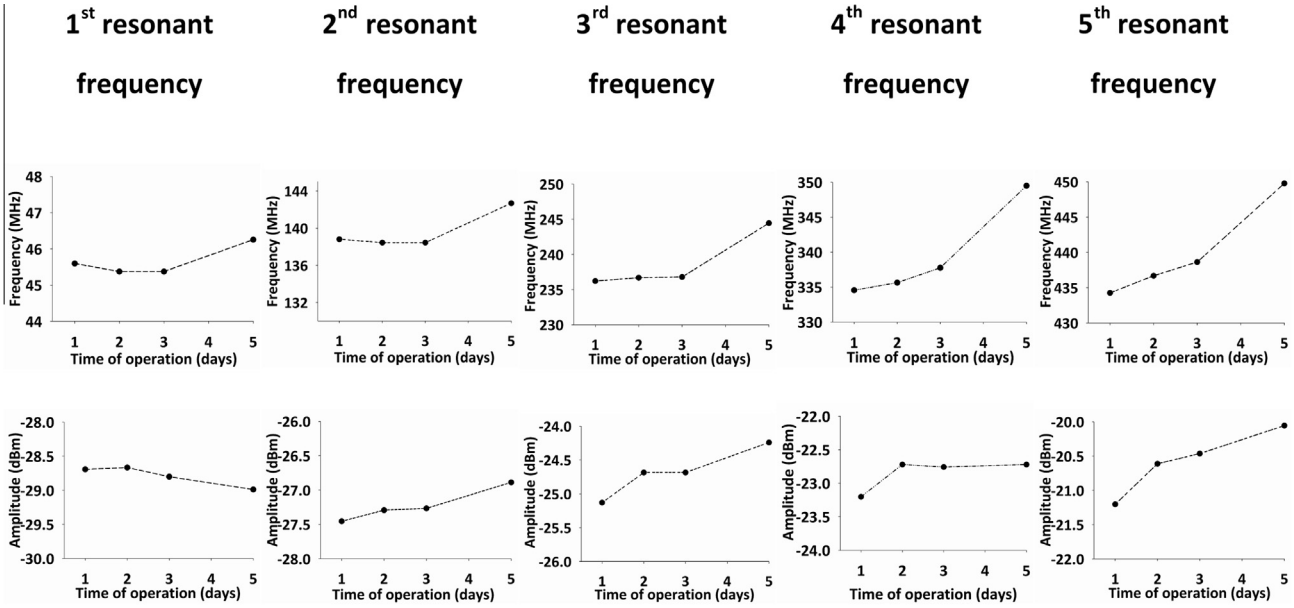

Fig. 15. Resonant frequency and amplitude of the first five resonances over a time period of four days and in response to AgCl deposition.

and 4, an effect possibly related to the observed mass starvation, as indicated by the data in Fig. 11, and subsequent blooming of the bacteria culture at day 4.

In order to relate the observed sensor response shown in Fig. 8 to the biofilm formation on the glass beads, model simulations were executed. Major objective was to investigate whether the changes in the AF responses, measured during the biofilm experiment, can be explained by changes in the dielectric properties of the composite material in the resonator, applying the model explained in Section 2.2.

A major challenge for the model simulations is to obtain a realistic estimate of the biofilm volume in the resonator, even more so because the % mass fraction of biomass in the biofilm strongly depends on process conditions. Reported values for the % mass fraction vary from 2% to 10%. [46,54–57]. For this reason, the model simulations were executed for these two limiting cases as well as for an assumed biomass fraction of 5%. The total amount of biomass in the biofilm and subsequently the volume fraction of biofilm were derived from the TOC measurements according to the procedure outlined in the "Supplementary information".

Table 4 gives an overview of the calculated volume fractions of the biofilm on the glass beads from day 1 to day 4 assuming biomass fractions (%) of the biofilm of 2%, 5% and 10%.

It should be mentioned that, as Table 4 shows, at the start of the experiment (i.e., the recording labeled day 1) a significant amount

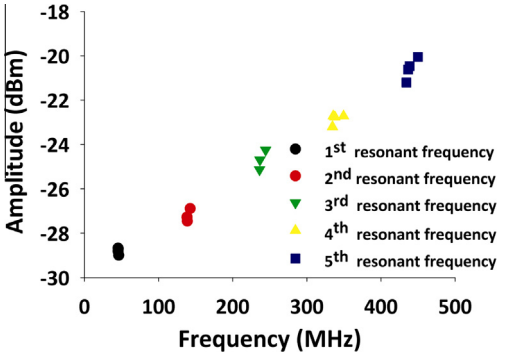

Fig. 16. Correlation between changes in resonant frequencies and amplitude for the first five resonances over a time period of five days and in response to AgCl deposition.

of TOC was measured already. Most likely, this TOC concentration represents small amounts of TOC originating from the feed substrate attached to the glass bead surface during sampling.

The two key parameters characterizing changes in the dielectric properties of the composite material in the resonator are ε_{re} and $\tan\delta_{eff}$. The biofilm consists of *E. coli* and EPS with relative dielectric constants of 60 and 70, respectively. In the simulations, it

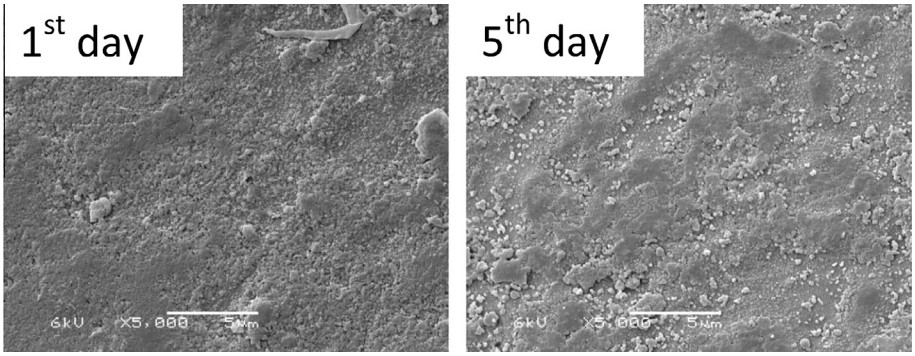

Fig. 17. SEM images of the glass bead surface before (left) and after (right) the deposition of AgCl.

was assumed that the dielectric constant of the biofilm layer $\varepsilon_l = 60$, thereby implicitly assuming that, at day 2, the dielectric properties of the biofilm are determined by the presence of *E. coli* rather than EPS (extracellular polymeric substance).

Fig. 13 shows the measured and simulated third resonance AF plots for the biofouling experiments using the biofilm volume fractions in Table 4, for days 1 and 2. Two models were compared, Lichtenecker's logarithmic law for composite material (model 1, Eq. (7)) versus a model description in terms of a system composed of parallel dielectric layers of glass, biofilm and feed substrate, respectively (model 2, Eq. (8)). As explained in Section 2.3, the "real life situation" is expected to represent an intermediate result between these two model simulations.

Both the experimental data and the model simulations reveal that biofilm formation on the glass beads results in a shift of the minimum in the AF plots towards higher frequencies. This is expected since, from an electrical point of view, biofilm formation can be seen as replacing feed substrate dielectric ($\varepsilon_m \sim 77$) by biofilm dielectric ($\varepsilon_l \sim 60$). As a result, biofilm formation will decrease the effective dielectric constant ε_{ceff}, resulting in a shift of the minimum in the AF plot towards higher frequencies, see also Eq. (3a) (representing the ideal resonator case, the applied model is described in more detail in [28]. Fig. 13 further shows that application of Lichtenecker's logarithmic law predicts a smaller shift of the AF plot towards higher frequencies than the "parallel dielectric layers" model, which results directly from the lower value of ε_{re} predicted by the "parallel dielectric layers" model.

In spite of the large number of assumptions made, both for calculation of the biofilm volume fraction in the resonator and for the model simulations, Fig. 13 clearly demonstrates that, in case of biofouling on the glass beads, the measured sensor response (shift in AF plot) is in the same direction and order of magnitude as predicted by the model, thereby confirming that the operating principle of the sensor is (predominantly) defined by changes of ε_{ceff}.

The results also reveal that a more detailed model, accounting for the exact geometric interactions between the different composite materials in the resonator, i.e., for the influence of glass beads with a shell of biofilm immersed in feed substrate on both dielectric permittivity and conductivity of the composite material, opens possibilities to use the model as a tool to relate signal change of the sensor more quantitatively to the volume fraction of biofouling in the system.

To further proof that the responses seen in Fig. 8 are indeed due to biofilm formation, a control experiment was performed in the presence of 3 mM/L of $AgNO_3$, a potent bacteria growth inhibitor (Fig. 14). The results are affirmative. Compared to Fig. 8, over the first 2 days the response hardly changed. Even though the response was clearly affected in a later stage (day 5), the observed shift was in opposite direction of the one seen in the absence of $AgNO_3$ in the feed solution, indicating quite a different working mechanism. This hypothesis was confirmed by Energy Dispersive X-ray spectroscopy (EDX) that identified the spots as depositions of AgCl, due to its low solubility (see also the "Supplementary information").

The AF responses of Fig. 15 were subjected to a similar analysis as those shown in Figs. 9 and 10. As in Fig. 9, the trend of the resonant frequency was identical for all resonances included in the analysis. As for the amplitude, we arrive at the same conclusion except for the first resonance. More importantly, the trends shown in Fig. 15 are essentially different from the one shown in Fig. 9. This distinction emphasizes the fact that the observed (shift in) response is due to a different cause, i.e., biofilm formation versus AgCl deposition, respectively.

Fig. 16 correlates the observed change in resonant frequency and the one in amplitude, for the first five resonances and over a time period of five days. The increasing dispersion at higher frequencies (resonances) is evident as the individual data points for each resonance diverge with increasing resonance number.

The difference between the glass bead surface covered with a biofilm and one with AgCl became also apparent from SEM images (Fig. 17). Whereas the images at day 1 of Figs. 12 and 17 are very similar, the images taken at day 4/5 are completely different with absolutely no bacteria cells attached in the presence of $AgNO_3$.

Note that the observed shift in the AF response curve towards higher resonance frequencies (see Fig. 14) is in the anticipated direction since the static relative dielectric permittivity ε_{eff} of AgCl is 11.14 [66], thereby decreasing ε_{eff} of the dielectric between inner and outer conductors, see equation Eq. (3a) and increasing the resonance frequencies of the resonator, see equation Eq. (3a).

4. Conclusions

- A flow-through stub resonator, with glass beads between inner and outer conductor as a surface for biofilm formation, was successfully applied to detect (early stages of) biofouling.
- Model simulations based on transmission line theory predict a shift in the amplitude versus frequency response of the sensor in the same direction and order of magnitude as observed experimentally, thereby confirming the operating principle of the sensor.
- The results indicate that isolated spots of biofilm and a homogenous biofilm layer result in a different AF response of the sensor, opening possibilities to discriminate between the onset of biofouling and a homogeneous biofilm layer
- The flow-through sensor design is relatively simple, robust and can be cleaned inline, opening possibilities to further develop it into a cost effective inline biofouling sensor.

Conflict of interest

The authors declare that there is no conflict of interest.

Acknowledgements

This work was performed in the TTIW-cooperation framework of Wetsus, Centre of Excellence for Sustainable Water Technology (www.wetsus.nl). Wetsus is funded by the Dutch Ministry of Economic Affairs, the European Union Regional Development Fund, the Province of Fryslân, the City of Leeuwarden and the EZ/Kompas program of the "Samenwerkingsverband Noord-Nederland". The authors thank the participants of the research theme Sensoring for the fruitful discussions and their financial support. Also authors are very grateful to Jelmer Dijkstra for help with SEM and EDX. Special thanks are also due to Tereza Rusková for her help with a large experimental part.

Appendix A. Supplementary data

Supplementary data associated with this article can be found, in the online version, at http://dx.doi.org/10.1016/j.sbsr.2014.10.012.

References

[1] H.-C. Flemming, Industrial Biofouling, Mater. Today 14 (11) (2011) 565.
[2] J. Wingender, H.-C. Flemming, Biofilms in drinking water and their role as reservoir for pathogens, Int. J. Hyg. Environ. Health 214 (6) (2011) 417–423.
[3] H.-C. Flemming, T. Griebe, G. Schaule, Antifouling strategies in technical systems – a short review, Water Sci. Technol. 34 (5–6) (1996) 517–524.
[4] H. Ivnitsky, D. Minz, L. Kautsky, A. Preis, A. Ostfeld, R. Semiat, C.G. Dosoretz, Biofouling formation and modeling in nanofiltration membranes applied to wastewater treatment, J. Membr. Sci. 360 (1–2) (2010) 165–173.
[5] A. Sweity, Y. Oren, Z. Ronen, M. Herzberg, The influence of antiscalants on biofouling of RO membranes in seawater desalination, Water Res. 47 (10) (2013) 3389–3398.
[6] S. Dürr, J.C. Thomason, Biofouling, Wiley-Blackwell, 2009.
[7] P. Henderson, Fouling and antifouling in other industries: power stations, desalination plants, drinking water supplies and sensors, Biofouling, Wiley-Blackwell, Chichester, 2010, pp. 288–305.
[8] H.-C. Flemming, Overview on fouling monitoring, in: Conference "Sensors4water", Assen, The Netherlands, 2013.
[9] T.R. Bott, D.M. Grant, Biofilms in flowing systems, Methods Enzymol. 337 (2001) 88–103.
[10] P. Janknecht, L.F. Melo, Online biofilm monitoring, Rev. Environ. Sci. Biotechnol. 2 (2–4) (2003) 269–283.
[11] E. Eguía, A. Trueba, B. Río-Calonge, A. Girón, J.J. Amieva, C. Bielva, Combinedmonitor for direct and indirect measurement of biofouling, Biofouling 24 (2008) 75–86.
[12] R.P. George, P. Muraleedharan, R.K. Dayal, H.S. Khatak, Techniques for biofilm monitoring, Corros. Rev. 24 (2006) 123–150.
[13] International Workshop Online sensors for fouling monitoring. Frankfurt am Main, Germany. http://events.dechema.de/Biofouling.html. November 29–30, 2010.
[14] L.F. Melo, T.R. Bott, Biofouling in water systems, Exp. Therm. Fluid Sci. 14 (4) (1997) 375–381.
[15] L. Tamachkiarow, H.-C. Flemming, On-line monitoring of biofilm formation in a brewery water pipeline system with a fibre optical device, Water Sci. Techn. 47 (2003) 19–24.
[16] E. Kujundzic, A. Cristina Fonseca, E.A. Evans, M. Peterson, A.R. Greenberg, M. Hernandez, Ultrasonic monitoring of early-stage biofilm growth on polymeric surfaces, J. Microbiol. Meth. 68 (2007) 458–467.
[17] J.S. Vrouwenvelder, M.C.M. van Loosdrecht, J.C. Kruithof, Early warning of biofouling in spiral wound nanofiltration and reverse osmosis membranes, Desalination 265 (1–3) (2011) 206–212.
[18] T. Piasecki, G. Guła, K. Nitsch, K. Waszczuk, Z. Drulis-Kawa, T. Gotszalk, Evaluation of *Pseudomonas aeruginosa* biofilm formation using Quartz Tuning Forks as impedance sensors, Sens. Actuators, B 189 (2013) 60–65.
[19] T. Ruiz, E.E. Lopez, J.A.G. Celis, S.G. Gomez, A.S. Abelleira, Chemical treatments against biofouling on industrial equipment associated with marine related power generation technologies, a new approach to an old problem, Oceans, IEEE, Spain, 2011, pp. 1–9.
[20] J. Klahre, H.C. Flemming, Monitoring of biofouling in paper mill process waters, Water Res. 34 (2000) 3657–3665.
[21] Y.W. Kim, S.E. Sardari, M.T. Meyer, A.A. Iliadis, H.C. Wu, W.E. Bentley, R. Ghodssi, An ALD aluminum oxide passivated surface acoustic wave sensor for early biofilm detection, Sens. Actuators, B 163 (1) (2012) 136–145.
[22] M. Fischer, M. Wahl, G. Friedrichs, Design and field application of a UV-LED based optical fiber biofilm sensor, Biosens. Bioelectron. 33 (1) (2012) 172–178.
[23] L. Pires, K. Sachsenheimer, T. Kleintschek, A. Waldbaur, T. Schwartz, B.E. Rapp, Online monitoring of biofilm growth and activity using a combined multi-channel impedimetric and amperometric sensor, Biosens. Bioelectron. 47 (2013) 157–163.
[24] P. Lens, V. O'Flaherty, A.P. Moran, P. Stoodley, T. Mahony, Biofilms in Medicine, Industry and Environmental Biotechnology Characteristics, Analysis and Control, IWA Publishing, London, 2003, ISBN 9781843390190, p. 608.
[25] R. Philip-Chandy, P.J. Scully, P. Eldridge, H.J. Kadim, M.G. Grapin, M.G. Jonca, M.G. D'Ambrosio, F. Colin, An optical fiber sensor for biofilm measurement using intensity modulation and image analysis, IEEE J. Sel. Top. Quantum Electron. 6 (5) (2000) 764–772, http://dx.doi.org/10.1109/2944.892616.
[26] J. Paredes, S. Becerro, F. Arizti, A. Aguinaga, J.L. Del Pozo, S. Arana, Interdigitated microelectrode biosensor for bacterial biofilm growth monitoring by impedance spectroscopy technique in 96-well microtiter plates, Sens. Actuators, B 178 (2013) 663–670.
[27] N.A. Hoog-Antonyuk, W. Olthuis, M.J.J. Mayer, D. Yntema, H. Miedema, A. van den Berg, On-line fingerprinting of fluids using coaxial stub resonator technology, Sens. Actuators, B 163 (2012).
[28] N.A. Hoog-Antonyuk, W. Olthuis, M.J.J. Mayer, H. Miedema, F.B.J. Leferink, A. van den Berg, Extensive modeling of a coaxial stub resonator for online fingerprinting of fluids, Procedia Eng. (2012) 310–313.
[29] N.A. Hoog, M.J.J. Mayer, H. Miedema, R.M. Wagterveld, M. Saakes, J. Tuinstra, W. Olthuis, A. van den Berg, Stub resonators for online monitoring early stages of corrosion, Sens. Actuators, B 202 (31) (2014) 1117–1136, http://dx.doi.org/10.1016/j.snb.2014.06.026. ISSN 0925-4005.
[30] M.J.J. Mayer, N.A. Hoog, RF antenna filter as a sensor for measuring a fluid, WO Patent 005084, 2011.
[31] M.J.J. Mayer, N.A. Hoog, Werkwijze en inrichting voor ingerprinting of het behandelen van een dielectricum in het algemeen en van water in het bijzonder, NL1038869, 16 (2012).
[33] D.M. Pozar, Microwave Engineering, Wiley, 2004.
[34] R.E. Collin, Foundations for Microwave Engineering, Wiley IEEE, 2000.
[35] N.A. Hoog, M.J.J. Mayer, H. Miedema, W. Olthuis, F.B.J. Leferink, A. van den Berg, Modeling and simulations of the amplitude-frequency response of transmission line type resonators filled with lossy dielectric fluids, Sens. Actuators, A 216 (1) (2014) 147–157, http://dx.doi.org/10.1016/j.sna.201. ISSN 0924-4247.
[37] B.M. Prakash, B.M. Veeregowda, G. Krishnappa, Biofilms: a survival strategy of bacteria, Curr. Sci. 85 (9) (2003) 1299–1307.
[38] R.M. Donlan, W.O. Pipes, T.L. Yohe, Biofilm formation on cast iron substrata in water distribution systems, Water Res. 28 (6) (1994) 1497–1503.
[39] Z. Lewandowski, J.P. Boltz, 4.15 – Biofilms in Water and Wastewater Treatment, Reference Module in Earth Systems and Environmental Sciences, from Treatise on Water Science, vol. 4, 2011, Current as of 15 March (2013) pp. 529–570.
[40] P. Stoodley, K. Sauer, D.G. Davies, J.W. Costerton, Biofilms as complex differentiated communities, Annu. Rev. Microbiol. 56 (2002) 187–209.
[41] I. Thome, M.E. Pettitt, M.E. Callow, J.A. Callow, M. Grunze, A. Rosenhahn, Conditioning of surfaces by macromolecules and its implication for the settlement of zoospores of the green alga Ulva linza, Biofouling 28 (2012) 501–510.
[42] W.G. Characklis, G.A. McFeters, K.C. Marshall, Physiological Ecology in Biofilm Systems in Biofilms, John Wiley & Sons, New York, N.Y., 1990, pp. 341–394.
[43] R. Jackson, P.F. Churchill, E.E. Roden, Successional changes in bacterial assemblage structure during epilithic biofilm development, Ecology 82 (2001) 555–566.
[44] I. Hanning, R. Jarquin, M. Slavik, *Campylobacter jejuni* as a secondary colonizer of poultry biofilms, J. Appl. Microbiol. 105 (4) (2008).
[45] H.-C. Flemming, Wingender J. Griegbe, C. Mayer, Physico-chemical properties of biofilms, in: L.V. Evans (Ed.), Biofilms: Recent Advances in Their Study and Control, Harwood Academic Publishers, Amsterdam, 2000, pp. 19–34.
[46] C. Dreszer, J.S. Vrouwenvelder, A.H. Paulitsch-Fuchs, A. Zwijnenburg, J.C. Kruithof, H.-C. Flemming, Hydraulic resistance of biofilms, J. Membr. Sci. 429 (2013) 436–447.
[47] M.S. Bhatnagar, Epoxy resins (overview), in: The Polymeric Materials Encyclopedia©, CRC Press Inc., 1996.
[48] Available from: http://bettly.ru/tabulky/relativni-permitivita.htm [in Russian].
[49] J. Naka, S. Yamamoto, K. Komori, S. Yamakawa, T. Kokubo, Development of glass fiber with high dielectric constant, J. Non-Cryst. Solids 177 (1994) 420–426.
[50] A. Dziaugys, J. Banys, V. Samulionis, J. Macutkevic, Y. Vysochanskii, V. Shvartsman, W. Kleemann, Phase transitions in layered semiconductor - ferroelectrics, in: M Lallart (Ed.), Ferroelectrics - Characterization and Modeling, InTech, 2011, ISBN 978-953-307-455-9, http://dx.doi.org/10.5772/20008.
[52] U. von Stockar, J.-S. Liu, Does microbial life always feed on negative entropy? Thermodynamic analysis of microbial growth, Biochim. et Biophys. Acta (BBA) – Bioenerg. 1412 (3) (1999) 191–211, http://dx.doi.org/10.1016/S0005-2728(99)00065-1. ISSN 0005-2728.
[54] W.-T. Tang, L.-Sh. Fan, Steady state phenol degradation in a draft-tube, gas-liquid-solid fluidized-bed bioreactor, AIChE J. 33 (2) (1987) 239–249, http://dx.doi.org/10.1002/aic.690330210. ISSN 1547-5905.

[55] W. Rauch, H. Vanhooren, P.A. Vanrolleghem, A simplified mixed-culture biofilm model, Water Res. 33 (9) (1999) 2148–2162, http://dx.doi.org/10.1016/S0043-1354(98)00415-1. ISSN 0043-1354.
[56] D.L. Chopp, M.J. Kirisits, B. Moran, M.R. Parsek, A mathematical model of quorum sensing in a growing bacterial biofilm, J. Ind. Microbiol. Biotechnol. 29 (6) (December 2002) 339–346.
[57] O.K. Lyngberg, C.P. Ng, V. Thiagarajan, L.E. Scriven, M.C. Flickinger, Engineering the microstructure and permeability of thin multilayer latex biocatalytic coatings containing E. coli, Biotechnol. Progr. 17 (6) (2001) 1169–1179, http://dx.doi.org/10.1021/bp0100979.
[58] Anna J. Svagan, My A.S. Azizi Samir, Lars A. Berglund, Biomimetic polysaccharide nanocomposites of high cellulose content and high toughness, Biomacromolecules 8 (2007).
[61] R. Späth, H.-C. Flemming, S. Wuertz, Sorption properties of biofilms, Water Sci. Technol. 37 (4–5) (1998) 207–210.
[62] J.W. Costerton, R.T. Irvin, K.-J. Cheng, The bacterial glycocalyx in nature and disease, Ann. Rev. Microbiol. 35 (1981) 299–324.
[63] P.H. Nielsen, A. Jahn, R. Palmgren, Conceptual model for production and composition of exopolymers in biofilms, Water Sci. Technol. 36 (1997) 9–11.
[66] Collaboration: Authors and editors of the volumes III/17B-22A-41B, Silver chloride (AgCl) refractive index, dielectric constants, in: II-VI and I-VII Compounds; Semimagnetic Compounds, vol. 41B, 1999, pp. 1–7.